System ID Modern Control Algorithms for Active Aerodynamic Load Control and Impact on Gearbox Loading*

Dale Berg, David Wilson, Brian Resor and Jon Berg
Sandia National Laboratories†
P.O. Box 5800, MS-1124
Albuquerque, NM USA
deberg@sandia.gov
dwilso@sandia.gov
brresor@sandia.gov
jcberg@sandia.gov

Thanasis Barlas
DUWIND, Delft University of Technology
Kluyverweg 1, Delft,
Netherlands
a.barlas@tudelft.nl

Ashley Crowther and Chris Halse
Romax Technology Ltd.
Rutherford House
Nottingham Science & Technology Park
Nottingham,NG7 2PZ
England
Ashley.Crowther@romaxtech.com
Chris.Halse@romaxtech.com

Abstract

Prior work on active aerodynamic load control (AALC) of wind turbine blades has demonstrated that appropriate use of this technology has the potential to yield significant reductions in blade loads, leading to a decrease in wind cost of energy. While the general concept of AALC is usually discussed in the context of multiple sensors and active control devices (such as flaps) distributed over the length of the blade, most work to date has been limited to consideration of a single control device per blade with very basic Proportional Derivative controllers, due to limitations in the aeroservoelastic codes used to perform turbine simulations. This work utilizes a new aeroservoelastic code developed at Delft University of Technology to model the NREL/Upwind 5 MW wind turbine to investigate the relative advantage of utilizing multiple-device AALC. System identification techniques are used to identify the frequencies and shapes of turbine vibration modes, and these are used with modern control techniques to develop both Single-Input Single-Output (SISO) and Multiple-Input Multiple-Output (MIMO) LQR flap controllers. Comparison of simulation results with these controllers shows that the MIMO controller does yield some improvement over the SISO controller in fatigue load reduction, but additional improvement is possible with further refinement. In addition, a preliminary investigation shows that AALC has the potential to reduce off-axis gearbox loads, leading to reduced gearbox bearing fatigue damage and improved lifetimes.

Keywords: active aerodynamic load control, smart blades, distributed control, dynamic simulation, gearbox fatigue life

1 Introduction

Reducing ultimate and oscillating (or fatigue) loads on wind turbine rotors can lead to reductions in loads on other turbine components such as gearboxes, generators and towers, resulting in large reductions in both the initial capital costs and the maintenance costs. These reductions, in turn, can lead to decreases in the resultant turbine cost of energy. With the ever increasing size of wind turbine blades and the corresponding increase in non-uniform loads along the span of those blades, the need for more sophisticated load control techniques has resulted in increased interest in the use of aerodynamic control devices (with associated sensors and control systems) distributed along each blade to provide feedback load control (often referred to in popular terms as 'smart structures' or 'smart rotor control'). A recent review of concepts and feasibility and an inventory of design options for such systems have been performed by Barlas and van Kuik at Delft University of Technology (TUDelft) [1]. Active load control utilizing trailing edge flaps or deformable trailing edge geometries (referred to here as Active Aerodynamic Load

† Sandia is a multiprogram laboratory operated by Sandia Corporation, a Lockheed Martin Company, for the United States Department of Energy's National Nuclear Security Administration under contract DE-AC04-94AL85000.

Control or AALC) is receiving significant attention, because of the direct lift control capability of such devices and recent advances in smart material actuator technology. Researchers at TUDelft [2-3], Risø/Danish Technical University Laboratory for Sustainable Energy (Risø/DTU) [4-10] and Sandia National Laboratories (SNL) [11-14] have been very active in this area over the past few years. TUDelft has focused mainly on investigating control concepts with analysis and experimentation, while Risø/DTU has focused heavily on analysis and experimental verification of actuator and control effectiveness. SNL, on the other hand, has performed extensive simulations of AALC on several turbine configurations and has analyzed the simulation results to estimate the fatigue damage reduction benefits of integrating morphing trailing edge technology into the tip region of the turbine blades.

2 Prior Simulations

2.1 Simulation Details

The vast majority of the simulation work to date has focused on utilizing a single sensor and a single control surface per blade. There is considerable interest in examining the potential benefits of measuring the loads or aerodynamic states and implementing control at multiple locations along the blade spans, but the available tools have not had sufficiently spatial resolution and/or aerodynamic load fidelity to support such simulations.

Turbine component fatigue accumulation calculations require time-series load histories at the turbine locations of interest at a number of mean wind speeds spanning the entire operating range of the turbine. The prior simulation work on AALC at Sandia has utilized the NREL FAST structural dynamics code [15], combined with the NREL Aerodyn aerodynamic code [16] to provide the aerodynamic forces on the blades. FAST utilizes a modal representation of the turbine to determine its response to applied forces; it models only the first and second flapwise bending and first edgewise bending blade modes, the first and second tower bending modes in fore-aft and side-to-side directions and drivetrain torsion.

All turbine simulations are driven with 10-minute duration, 3-dimensional turbulent wind fields (IEC Normal Turbulence Model, Type B turbulence [17]); at least six simulations with different wind fields are run at each mean wind speed to develop representative load distributions. The simulations span the range of mean wind speeds from cut-in to maximum wind shut down.

The critical turbine location load-time histories are rain-flow cycle counted with the NREL Crunch code [18] and these results are used in linear damage calculations to determine the fatigue damage accumulation for each mean wind speed at each of the critical turbine locations. Combining those accumulations with a Rayleigh wind speed distribution for a mean wind speed of interest yields an overall damage accumulation for each turbine location for that particular mean wind speed. The impact of the AALC addition to the baseline rotor is also evaluated by examining the ratios of damage equivalent load (DEL) at the critical locations for the modified rotor to the DEL at those same locations for the baseline rotor. A decrease in DEL represents a decrease in the overall fatigue damage in the structure and a resulting increase in fatigue life.

2.2 Turbine Model

The wind turbine analyzed in this work is the NREL/Upwind 5MW turbine [19], a conceptual machine that is representative of utility-scale land- and sea-based multi-megawatt turbines. It is a conventional three-bladed, upwind, variable-pitch, variable-speed turbine that was selected because the details of the model are available in the open literature. Table 1 summarizes some of the basic properties of the turbine.

Rating	5.0MW
Rotor Size	126m
Blade Length	61.5m
Hub Height	90m
V_{rated}	11.4m/s
$V_{cut\text{-}out}$	25m/s
AALC Device	Conventional flap (10% chord)
Extent of AALC	25% of blade (from 67% to 92% of blade span)
Deflection limits	+/- 10°

Table 1. 5MW Wind Turbine Characteristics.

2.3 Results and Limitations

The prior simulation work presented in [11-14] used a simple Proportional-Derivative (PD)

controller to minimize the deflection of each blade tip from its nominal location. Table 2 and Figure 1 compare the one-million cycle DEL of the 5MW rotor with AALC to the baseline rotor (without AALC). Adding AALC devices resulted in significant decreases in blade-root flap, tower-base fore-aft and tower-top yaw moment fatigue damage across all wind speeds, with essentially no effect on blade-root edge and tower-base side-side moment fatigue damage. While the low-speed shaft torque fatigue damage increased a relatively large amount at the higher wind speeds, the overall change across all wind speeds for this particular turbine/controller configuration was relatively small (7.5% and 14.5% for Rayleigh distributions of 5.5m/s and 7m/s, respectively). In addition, the actual baseline fatigue damage for the shaft torque is at least eight orders of magnitude below that of any other location, with the exception of the blade root pitch moment.

One-million Cycle Damage Equivalent Load (AALC/Baseline)					
	9m/s	11m/s	18m/s	Rayleigh Wind 5.5m/s	Rayleigh Wind 7m/s
Low Speed Shaft Torque	2.1	17.7	27.0	7.5	14.5
Blade Root Edge Moment	2.3	3.0	-0.1	1.5	1.6
Blade Root Flap Moment	-34.0	-14.2	-13.6	-15.3	-14.3
Blade Root Pitch Moment	-0.8	7.9	27.6	7.7	12.0
Tower Base Side-Side Moment	3.9	0.5	-5.5	-0.6	-3.3
Tower Base Fore-Aft Moment	-24.3	-12.7	0.1	-4.9	-6.2
Tower Top Yaw Moment	-32.4	-10.5	-17.4	-13.8	-15.9

Table 2. Changes to Fatigue Damage Accumulation Resulting from the Addition of Morphing Trailing Edge Technology to 5MW NREL Offshore Turbine. Trailing Edge Flap is 20% Chord, +/-10° Maximum Deflection, 100°/sec Deflection Rate Limit. All Damage is % Change from the Baseline Levels.

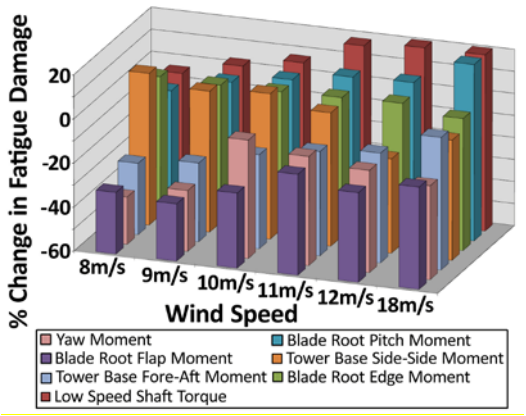

Figure 1. Changes to Fatigue Damage Accumulation Resulting from the Addition of Morphing Trailing Edge Technology to 5MW NREL Offshore Turbine. Trailing Edge Flap is 20% Chord, +/-10° Maximum Deflection, 100°/sec Deflection Rate Limit. All Damage is % Change from the Baseline Levels.

One way to assess the potential impact of such a decrease in the blade-root bending moment on the turbine cost of energy is through the "Grow the Rotor" analysis presented by Berg, et al in references 12 and 13. For a 1.5MW turbine, the addition of AALC lowered the blade-root bending moment fatigue damage sufficiently to permit a 10% larger diameter rotor to be placed on the existing drive train and tower, resulting in a 5 to 9% decrease in turbine cost of energy, depending on site-average wind speed, as shown in Figure 2 [from 13]. Obviously, these results depend heavily on the estimated costs associated with the addition of AALC – those are itemized in Berg, et al [13]. A much more detailed analysis and major design studies would be required to determine the actual improvements in cost of energy that might be realized.

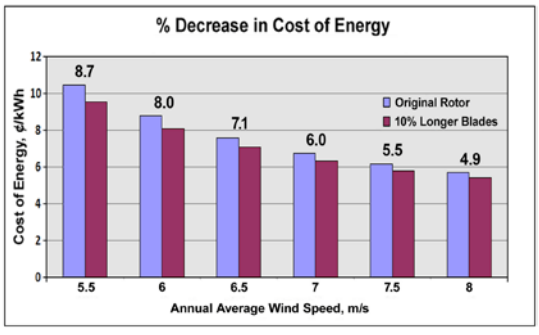

Figure 2. Impact of 10% Growth in Blade Length on the Cost of Energy for the WindPACT 1.5MW Turbine with AALC. MorphingTrailing Edge with 20% Chord, +/-10° Maximum Deflection, 100°/sec Deflection Rate Limit.

This prior work suffers from several inaccuracies in the modeling of the wind turbine and the AALC devices. The FAST/Aerodyn simulation tool was developed to accurately model conventional turbines without active control surfaces. It simply is not adequate for investigating the impact of rapidly deploying and retracting distributed trailing edge control surfaces. These inaccuracies include, but are not limited to:

- Aerodyn suffers from inaccurate wake models and inaccurate models of the unsteady effects of activating blade trailing edge flaps.
- The spatial modeling resolution of FAST is not adequate to simulate the loading on and response of a blade with several independent load control devices distributed along the trailing edge of the blade.
- The AALC control was limited to a very basic PD controller.

3 Current Simulation Work

3.1 Simulation Details

In the current controller development work described in this section, the required time-series load histories are generated with structural dynamic simulations of the turbine performed with the DU_SWAMP (Delft University Smart Windturbine Aeroelastic Modular Processing) aeroservoelastic code [20]. DU_SWAMP offers potential for higher numbers of structural modes than what is available in FAST, and utilizes non-linear structural modeling, in contrast to the modal representation of the structure used in FAST. It also incorporates realistic time-dependent aerodynamic effects for distributed trailing edge flap actuation and allows for rapid and easy design and implementation of real time controllers via Simulink©. Sandia and TUDelft have recently validated DU_SWAMP against the NREL FAST/Aerodyn code and other codes; details may be found in the paper by Resor, Wilson, Berg, Berg, Barlas and van Kuik [21].

As mentioned earlier, FAST models only the first and second flapwise bending and first edgewise bending blade modes, as well as first and second tower bending modes in fore-aft and side-to-side directions. The DU_SWAMP model used in this work contains two superelements and represents the first mode in each orthogonal direction for both the tower and blades; it represents the second and third and modes in each direction for both the tower and blades with reduced accuracy. After the work presented here was completed, a three superelement model that accurately represents the first and second modes in each direction for the blade and tower and represents the third and forth modes with somewhat reduced accuracy became available. Future work will investigate the impact of that higher resolution model on these results. The drive train dynamics, tower shadow, structural torsion in the blades and tower and aerodynamic hub losses can be modeled in DU_SWAMP, but are not included in the current investigation.

The wind turbine analyzed in this work is the NREL/Upwind 5MW turbine, the same turbine as was analyzed in the prior simulation work, with the properties listed in Table 1.

3.2 System Identification Effort

The closed form linearized aeroelastic equations that describe this system are not readily available, so utilizing the eigenvalue approach is not a viable method for determining the aeroelastic modes and their frequencies. System identification is performed in order to understand which modes are actually present in the model and what their frequencies are; this technique can also be utilized later on a real turbine in the field. Three virtual vibration test scenarios are performed in order to identify the modes.

First, the blade or tower structure is isolated in Simulink with cantilevered base boundary condition and aerodynamic forces are removed. The free tip of the structure is excited with an input force in a "virtual vibration test." The input force waveform consists of a logarithmic chirp, a sinusoidal input with frequency varying logarithmically in time. The log-chirp has been shown to be an efficient waveform to exciting low frequency, highly damped modes as well as high frequency modes using minimal simulation time. These input forces and the associated structural responses are used to generate a frequency response function, from which the structural modes of the blades and tower are identified from the spectrum peaks.

Second, the active aero enabled blades are placed on a rigid spinning hub. The hub is constrained in all degrees of freedom except for shaft revolution. Aerodynamic forces due to a steady 15 m/s wind input are applied and the turbine is allowed to spin up to steady operating conditions. System identification of the aeroelastic modes of the spinning blades is performed with the aid of active flaps driven by the log-chirp waveform. In this case, all flaps are driven with equal deflection and phase. Additional combinations of flap

phasing would identify additional asymmetric modes of the aeroelastic system. It is important to note that at this stage of virtual testing on this system we find very pronounced effects of aerodynamic damping on the structure; this damping tends to reduce the appearance of distinct structural modes in the system response. As an example, the first collective flap mode is not clearly detected for the 15 m/s wind input. The mode is detected for a 7 m/s steady wind input and is indicated in Table 3.

Finally, the previous aeroelastic identification with log-chirp flap aerodynamic excitation is repeated on the full turbine system, including tower flexibility.

*Two frequencies for modes of similar behavior are shown.

	1) Isolated structure, cantilevered, frequency (Hz)	2) Three blades on rigid hub , shaft revolution only, frequency (Hz)	3) Entire Turbine, Frequency (Hz)	From [Jonkman, et al, Table 9-1] (Hz)
Blade 1st Flap	0.69	0.62 @ 7m/s		0.6993
Blade 2nd Flap	3.51	3.6-3.7	3.4-3.8	2.0205
Blade 3rd Flap	11.44	10.4 11.6*	10.4 11.6*	NA
Blade 1st Edge	1.07	1.08	1.09	1.0793
Blade 2nd Edge	5.41	5.42	5.42	NA
Blade 3rd Edge	17.5	19.6	19.6	NA
Tower 1st F-A	0.26			0.3240
Tower 2nd F-A	2.15		2.12	2.9003
Tower 1st S-S	0.26		0.22	0.3120
Tower 2nd S-S	2.16		2.12	2.9361

Table 3. Elastic and aeroelastic system identification results.

3.3 Controller Development

In an earlier paper Wilson [22] describes a system identification approach and model development procedure that can be employed for distributed control system design for large wind turbine load reduction applications. A process is outlined that can be used with multiple sensor inputs and actuator outputs of varying types to construct state-space models compatible with MIMO modern control techniques such as LQT, LQG, H_∞ and robust control.

Prior work by Andersen et al [5] investigated the impact of utilizing multiple independent flaps, rather than a long single flap on each rotor blade. That work utilized multiple independent classical PD controllers with gains tuned as necessary to ensure that the controllers do not oppose each other. This work, in contrast, utilizes a modern control approach with a single MIMO controller. The 5MW reference turbine example used in this paper demonstrates the overall control law design procedure for the SISO and MIMO LQR flap controller blade load reduction.

The DU SWAMP aeroservoelastic simulator is employed to evaluate the above distributed flap control system performance and validate the procedure for developing aeroservoelastic computational models for distributed control system design. The performance is tested with a 15 m/s wind condition (maximum power operation). The three dimensional wind input is generated by TurbSim [23] with 6% turbulence intensity generated according to the Kaimal spectrum. Six percent turbulence intensity is low compared to typical standards but is chosen in order to ensure the highest reliability of longer simulation runs by DU SWAMP. During the control evaluation 400-second time segments were used. The excitation flap input data used by Wilson [22] is used along with the addition of a sinusoidal sine chirp to identify the model. This model is then used in the SISO and MIMO controller designs. However, only single flap excitation data is used for the SISO design while multi-flap

excitation data is also included for the MIMO design. The SISO data effectively identifies the first two blade flap modes in Table 3 while the MIMO data captures all three of those blade flap modes. The MIMO design allows for independent variation of the three flaps on the blade, while the SISO design treats all three flaps on the blade as a single flap input. All three local flapwise velocity signals (which can be readily measured on an actual turbine with accelerometers) are used for the MIMO design while only the middle local flapwise velocity is used as the feedback signal for the SISO design. Note that this is an initial design for these controllers; further development will undoubtedly result in improved designs.

Figure 3 shows the equivalent damage loading for a SISO LQR flap controller design (top) and for a MIMO LQR flap controller design (bottom). The results for a conventional tip deflection rate feedback control design and the LQR controller designs are shown in Table 4. While the SISO design performs better than the conventional controller, the MIMO design provides further refinement and lower DEL values. These results show less load reductions than the conventional PD control results found in Resor [21], but that work focused on tip deflection reduction. The goal of this study is to explore the need for a refined MIMO flap controller design to better suppress load fluctuations due to varying wind conditions. This can also be a factor as the blades increase in size and become lighter for larger wind turbines (10MW, 15MW). One benefit of the MIMO controller design is that a nominal reference point (required for the PD control in reference [21]) is not required, since a local deflection rate feedback signal is employed. Further investigation of combinations of system identification models, sensor measurements, and actuator types and locations can influence and change the performance of the control system as part of future work.

Representative time domain responses for blade 1 flap root moments and blade flap local deflection are compared to the baseline case (no AALC control) in Figures 4 and 5 for both the SISO and MIMO LQR flap controller designs. Examination of the spectra for the flap root moment response presented in Figure 6 reveals that, while the response at frequencies in the vicinity of the first blade flap mode (0.7 Hz) has been decreased by the controllers (and the MIMO is more effective than the SISO in this regard), the response near 2Hz and 3.8Hz (the second blade flap mode) has been increased significantly. The spectra for the blade flap local deflection shows nearly identical results. Clearly additional development of these controllers is required to decrease the flap root moment response across all frequencies.

Figure 7 illustrates the SISO (top) and MIMO (bottom) LQR Flap controller deflection inputs. The MIMO controller clearly shows the distinct individual flap deflection commands.

	Waveform standard deviation reduction (%)	DEL reduction (%), m=10, Fiberglass	DEL reduction (%), m=3, Steel
Tip Rate Control	8.7	10.9	11.4
SISO Control	11.3	11.8	13.4
MIMO Control	18.1	17.0	18.8

Table 4. Comparison of PD, SISO and MIMO Control Impacts on Blade Root Flap Bending Moment. 15 m/s, 6% Turbulence.

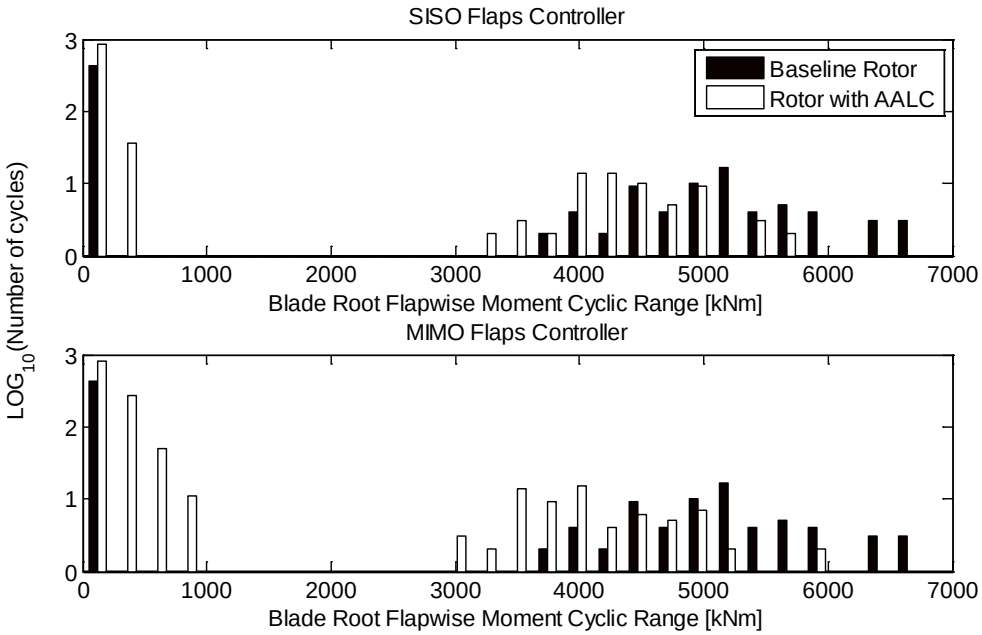

Figure 3. Cyclic Load Amplitude Spectra for SISO LQR Flap Controller (top) and MIMO LQR Flap Controller (bottom). 15 m/s, 6% Turbulence.

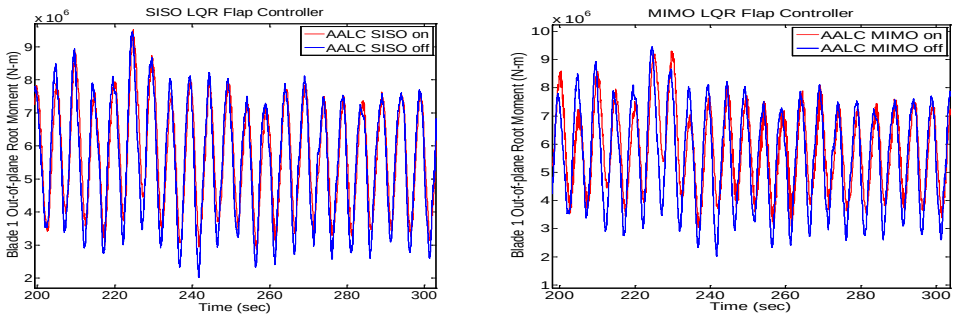

Figure 4. Blade 1 Root Flap Moment Response for SISO (left) and MIMO (right) Controllers, Both Compared to Baseline (no AALC) Case. 15 m/s, 6% Turbulence.

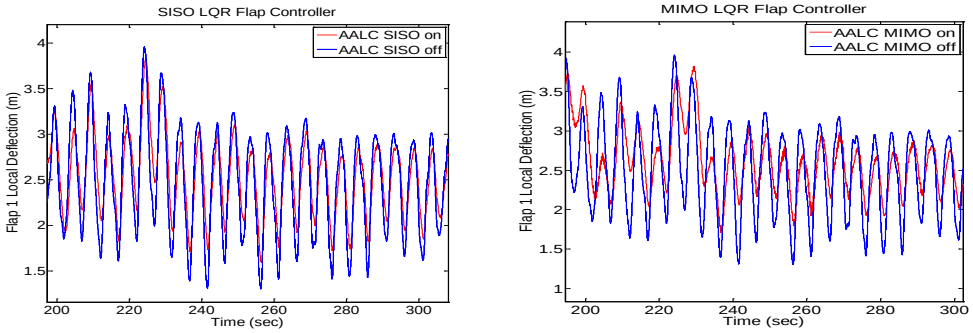

Figure 5. Blade 1 Deflection at the Flap Location for SISO (left) and MIMO (right) Controllers, Both Compared to Baseline (no AALC) Case. 15 m/s, 6% turbulence.

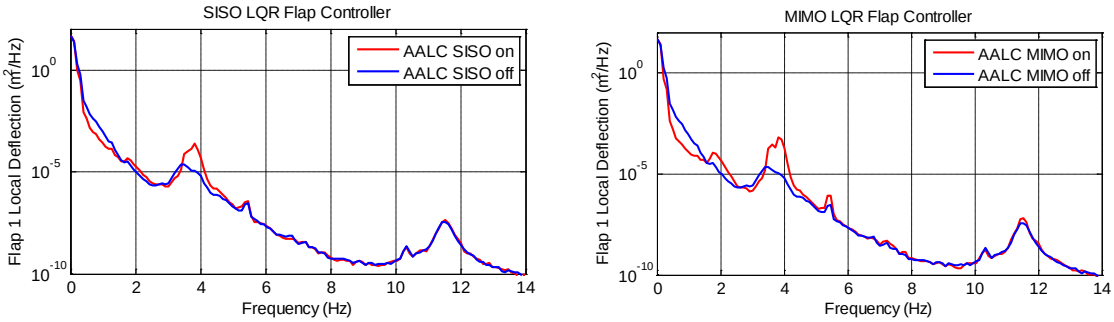

Figure 6. Specta of the Root Flap Moment Response for SISO (left) and MIMO (right) Controllers. 15 m/s, 6% Turbulence

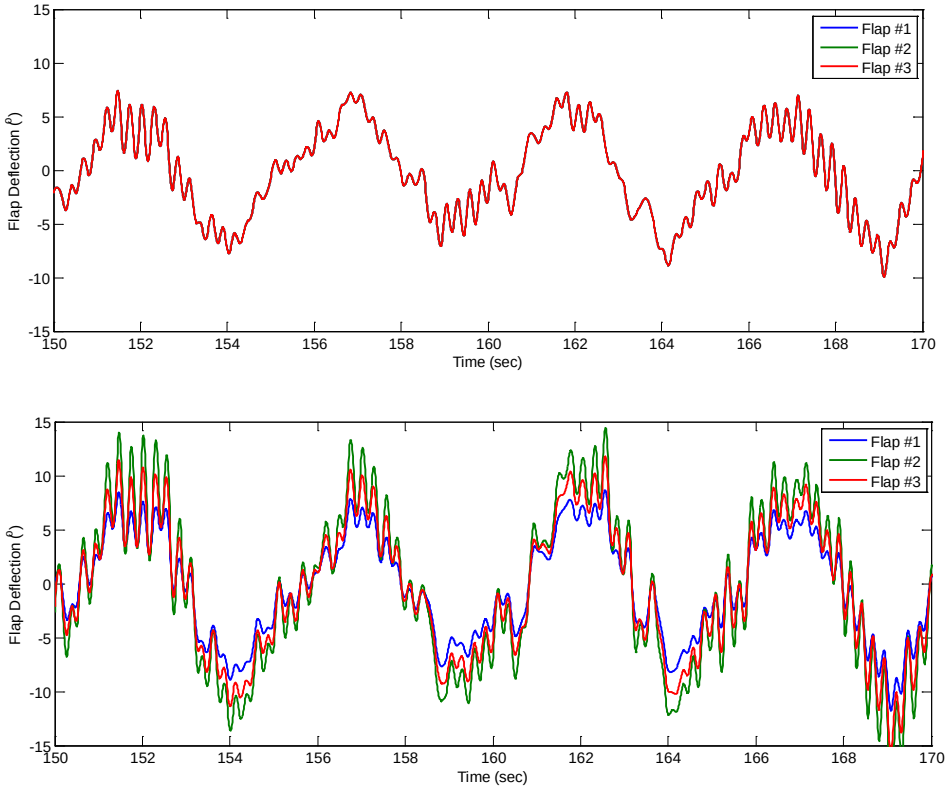

Figure 7. Blade SISO (top) and MIMO (bottom) LQR Controller Flap Deflection Commands. (Note the same command to all three flaps for the SISO controller.) 15 m/s, 6% turbulence.

4 Impact of Active Aero Load Control on Gearbox Fatigue Loading

To this point in time, only the impact of AALC on blade fatigue loading and damage has been investigated. However, initial discussions between SNL personnel and representatives of Romax Technology, who have extensive experience in detailed analyses of gearboxes, led to the idea that the use of AALC may also lead to reductions in damaging gearbox loads. Romax performed a limited analysis utilizing a 1.5MW gearbox model that they had previously developed and 1.5MW turbine AALC simulation data generated by SNL in conjunction with the work reported in Berg el al [12] to further investigate this idea. This AALC simulation data was generated with the FAST/Aerodyn code.

A model of a typical 1.5MW drive-train design is used for this analysis. The gearbox has a total ratio of 95:1 and a design lifetime of 20 years. The gearbox arrangement is a single planetary stage and two parallel helical gear stages. The drive-train layout is a “three-point mounted” design, with one main-shaft bearing and an elastomeric mount connected to the torque arms of the gearbox. The main shaft bearing acts as a pivot point in such designs and a proportion of the off-axis loads are transmitted to the gearbox housing through the planet carrier bearings and reacted at the

gearbox mounts. The main bearing is a double row taper roller and provides a supporting moment given its tilt stiffness. The planet carrier is supported by two taper roller bearings. Other designs may include a second main-shaft bearing to react off-axis loads and further isolate the gearbox, but the cost and space requirements for the second main bearing must be balanced against the reductions in the loads on the gearbox.

Some key features of the model include beam finite element representation of shafts, solid finite element representation of gearbox housing, gear blanks, planet carrier and torque arms and 6DOF spring connections for (elastomeric) trunnion mounts. The gears and bearings are modeled with semi-analytical formulations that take account of important factors such as misalignment, area of contact under load, gear and bearing microgeometry, radial and axial clearances or preload and material properties. Quasi-static non-linear analysis can be performed for prescribed loading conditions; the global deflections are solved simultaneously with the contract mechanics for the gears and bearings. Thus the effect of the whole system behaviour on contact elements is captured. Designers use these models for achieving good alignment of the system under the loads, calculating gear and bearing contact stress and life, optimizing the microgeometry of the gears for increased life and transmission error and predicting the gear vibration magnitudes, as well as for many other purposes. The model of Figures 8 and 9 does not include the flexibility of the bedplate system between the main bearing and the gearbox mounts (although this may be included). The outer race of the main bearing is grounded, as are the gearbox mounting pins (the gearbox mounts do, however, have flexibility). It is assumed here that the high speed shaft connection between the generator and the gearbox cannot carry any load except torque, so the generator is modelled as a pure torque output from the system.

The aim of the analysis is to evaluate the improvement in extreme deflections of this drivetrain due to the implementation of the AALC. To that end simulation data was produced describing the load on the hub in all directions (3-dimensional forces and moments) due to normal operating conditions, with turbulence, with and without AALC. Six 600 second time histories were produced for the AALC and baseline cases. Again, the AALC simulation data used in this investigation was existing data from an earlier study, and the controller was designed to minimize blade-tip deflection; it was not designed to impact the loading on the gearbox! We would anticipate that a controller tuned to reduce the off-axis gearbox loads would show even larger impact than that presented here.

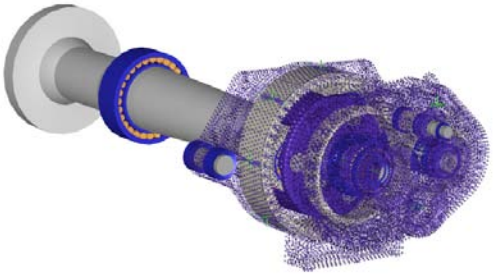

Figure 8. RomaxWind drivetrain model for 1.5MW wind turbine generator

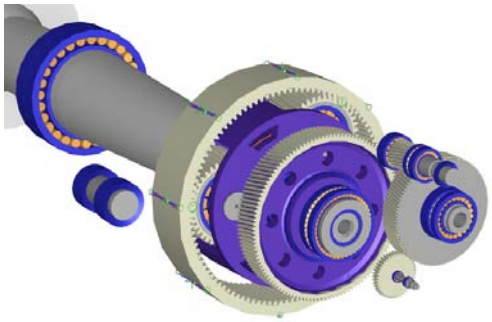

Figure 9. RomaxWind drivetrain model showing the single stage planetary and two parallel stage gearbox arrangement

One effect of the AALC is to reduce the off-axis loading, such as side loads and over-turning moment. There is also a redistribution of the driving torque that will affect the durability of gearbox components, which we do not consider here. The change in the extent of the simulated loads can be seen in Figure 10. The simulations without AALC are named the “baseline” cases. This figure shows that the mean values have not changed significantly between the baseline and AALC cases, but the range over which the off-axis loads vary, particularly for the M_y and M_z directions, is reduced significantly by the AALC (see Figure 11 for a definition of the coordinate system).

As a preliminary investigation into the effect on the system durability we can calculate the stress due to a set of load cases with the maximum hub force and moment as defined in Table 5, similar to an extreme load analysis. The load cases are all based on the mean values above, and then each load direction is varied individually to its maximum and minimum values.

The system deflection is calculated for each of the cases, including the effects of all the flexible elements in the model. An illustration of a static result is shown in Figure 12; the deflection of the mainshaft across the main bearing can be readily seen.

The change in gear stresses due to the off-axis loading is small, indicating that the increased off-axis loads are being supported effectively by the bearings and they are not introducing significant changes in misalignment at the gear teeth. The changes in bearing loads and misalignment are more significant. The effect on the carrier bearings is illustrated in Figure 13, where the ISO equivalent load (a measure of the total axial and radial load on the bearing) and the bearing misalignment are presented. It is clear from this figure that the load on the carrier bearings changes most significantly due to the extreme loads M_y and M_z (moments about the y-axis and z-axis respectively). Figure 14 and 15 show calculated contact stress on the bearing outer raceways for the two situations. Here we can see the contact is still distributed reasonably well along the tapered roller's lengths, but the contact stress is higher in the baseline case due to the increased load. The increased magnitude of the stress cycles that the bearings undergo will increase the damage to the bearings and reduce their life. This study suggests that the AALC will have particular uses in mitigating drivetrain damage due to the high off-axis loads that the bearings otherwise have to support.

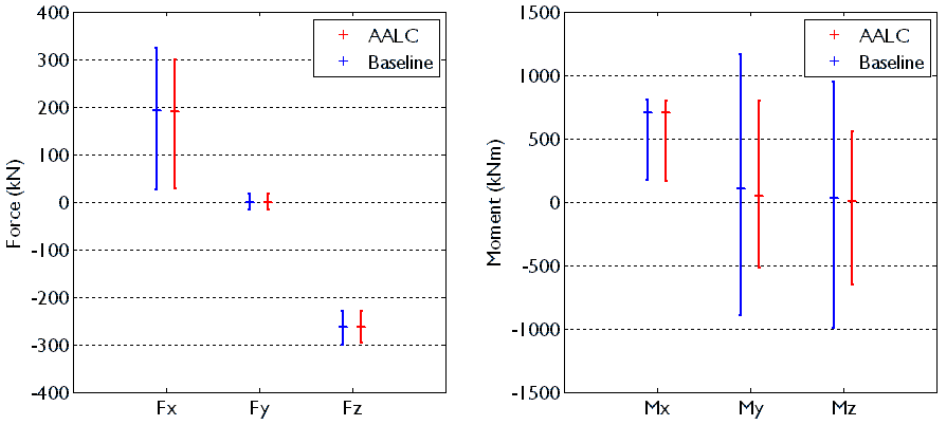

Figure 10. Mean and maximum and minimum hub loads in all directions from baseline and AALC time histories.

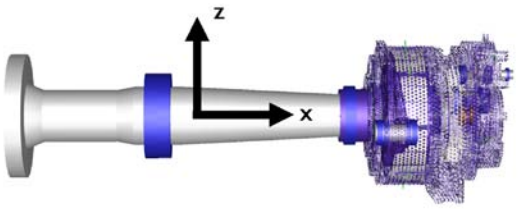

Figure 11. Coordinate system used. X is along the axis of the mainshaft pointing downwind. Z is perpendicular to the axis of the mainshaft upwards. Y makes a right-handed coordinate system (into the page in the figure).

Force	Symbol	Unit	AALC			Baseline		
			Mean	Min	Min	Min	Mean	Max
Force in X direction	F_x	kN	189.3	26.4	26.4	26.4	189.3	299.6
Force in X direction	F_y	kN	-1.0	-17.7	-17.7	-17.7	-1.0	15.6
Force in X direction	F_z	kN	-262.3	-301.5	-301.5	-301.5	-262.3	-230.3
Moment about X-axis	M_x	kNm	701.5	171.5	171.5	171.5	701.5	793.1
Moment about Y-axis	M_y	kNm	48.4	-898.6	-898.6	-898.6	48.4	793.2
Moment about Z-axis	M_z	kNm	2.8	-999.9	-999.9	-999.9	2.8	557.7

Table 5. Extreme loads from simulations

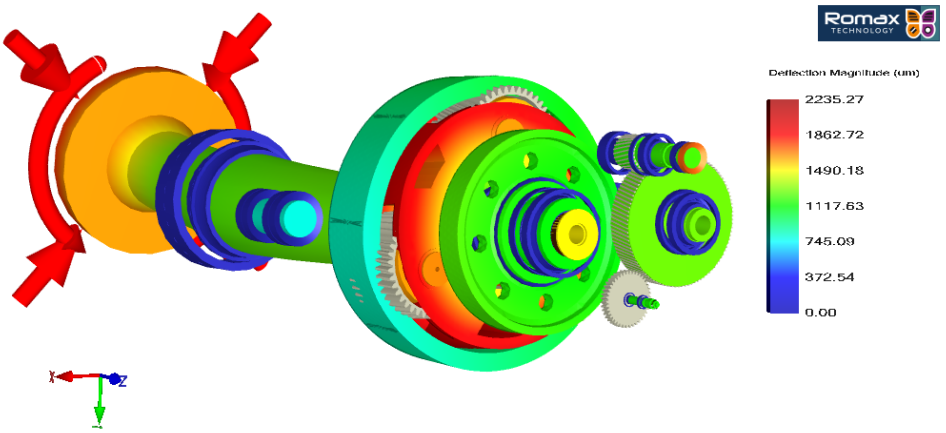

Figure 12. Static deflection of system to Baseline $M_{y,max}$ load case, housing not displayed.

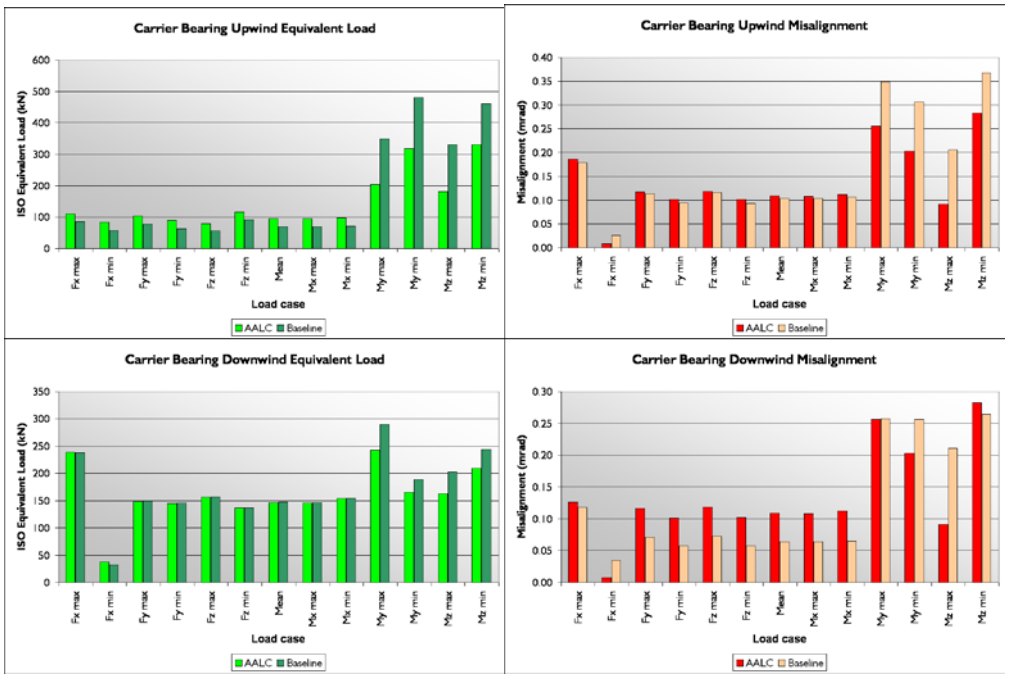

Figure 13. Bearing equivalent load and misalignment for extreme loads

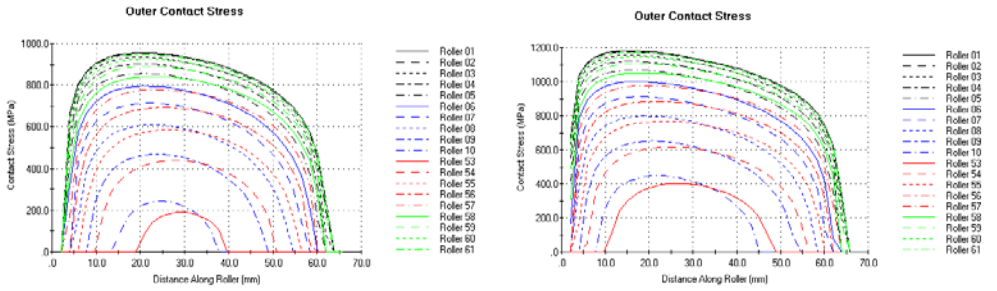

Figure 14. Carrier Upwind Bearing, AALC $M_{y,max}$ (left), Baseline $M_{y,max}$ (right)

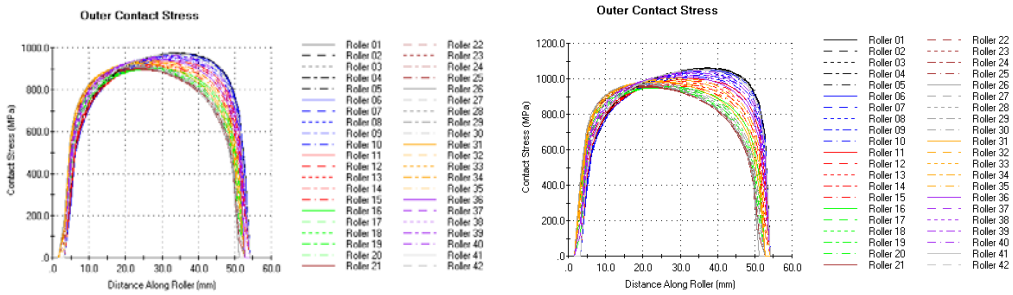

Figure 15. Carrier Downwind Bearing, AALC $M_{y,max}$ (left), Baseline $M_{y,max}$ (right)

5 Summary and Future Work

Techniques for system identification of the operational aeroservoelastic wind turbine in stochastic inflow have been evaluated. The work presented here has demonstrated the need for thorough characterization of the operating, aerodynamically loaded wind turbine system. The operational modes of the wind turbine are found to be different from what can be measured on the parked turbine system due to effects of rotor rotation and aerodynamic loads and damping. Measurement of the operational modes with the use of the appropriate rotor excitation (which may include, but are not limited to, individual flap actuations and blade pitch actuations) will enable better controller design. The initial SISO and MIMO controllers developed with these techniques are far from optimum and must be further developed. The nature of the ideal input signal for exciting these rotor actuations is still to be determined.

In the context of control system design, the control performance is tied directly to the accuracy of the identified model. Properly identified state-space models are compatible with a whole regime of MIMO modern control techniques (LQR, LQG, H1, μ-synthesis, loopshaping, uncertainty modeling, multivariable stability margins, etc., along with other robust control concepts) can now be applied. Many of these modern control design techniques are performed with respect to a performance index or cost function. The cost function can be designed for efficient and robust operation (with respect to a changing environment) of blade AALC strategies and integration with a smart health monitoring system and overall wind turbine control system architecture.

Further investigations of load reduction under varying wind conditions using distributed flaps and various combinations of sensor measurements can be assessed. Studies of multiple flaps, flap spanwise locations, and sensor measurements (structural: strain, strain-rate, tip deflection, accelerometers, etc. and aerodynamic: pressure, pitot-tube, etc.) can now be conducted to help identify promising active aerodynamic load control techniques. Trade-off studies of loads reduction and effects on energy capture will help develop the smart wind turbine system with optimized performance for the future.

The preliminary analysis of the impact of AALC on gearbox loads suggests that AALC may indeed be useful in mitigating off-axis gearbox loads and reducing gearbox fatigue damage. Further studies are needed to quantify the amount of this reduction and to investigate the extent to which this fatigue can be mitigated when the controller is designed with this objective in mind.

References

[1] Barlas, T.K. and van Kuik, G.A.M., Review of state of the art in smart rotor control research for wind turbines, *Progress in Aerospace Science (2009)*, doi:10.1016/j.paerosci.2009.08.002

[2] Troldborg, N., Computational study of the Risø B1-18 airfoil with a hinged flap providing variable trailing edge geometry. *Wind Engineering* 2005, 29:89-113.

[3] Buhl, T., Gaunaa, M., and Bak, C., "Load reduction potential using airfoils with variable trailing edge geometry," *Proceedings of the 43th AIAA/ASME*, Reno, NV, USA, 2005.

[4] Buhl, T., Gaunaa, M., and Bak, C., Potential load reduction using airfoils with variable trailing edge geometry. *Solar Energy Engineering* 2005, 127:503-16.

[5] Andersen, P. B., Gaunaa, M., Bak, C., and Buhl, T., "Load alleviation on wind turbine blades using variable airfoil geometry," *Proceedings of the EWEC* 2006, Athens, Greece.

[6] Andersen, P. B., Gaunaa, M., Bak, C., and Buhl, T., "Wind tunnel test on wind turbine airfoil with adaptive trailing edge geometry," *Proceedings of the 45th AIAA/ASME*, Reno, NV, USA, 2007.

[7] Buhl, T., "Stability Limits for a Full Wind Turbine Equipped with Trailing Edge Systems," European Wind Energy Conference, Marseille, France, 16-19 March, 2009.

[8] Anderson, P.B., "Load Reduction Using Pressure Difference on Airfoil for Control of Trailing Edge Flaps," European Wind Energy Conference, Marseille, France, 16-19 March, 2009.

[9] van Wingerden, J-W., Hulskapp, A.W., Barlas, T., Marrant, B, van Kuik, G.A.M., Molenaar, D-P, and Verhaegen, M., On the Proof of Concept of a 'Smart' Wind Turbine Rotor Blade for Load Alleviation, Wind Energy, 2008; 11:265-80.

[10] Barlas, T., van Wingerden, J-W, Hulskamp, A, and van Kuik, G, "Closed-loop Control Wind Tunnel Tests on an Adaptive Wind Turbine Blade for Load Reduction," *Proceedings of the 46th AIAA/ASME*, Reno, NV, USA, 2008.

[11] Wilson, D.G., Berg, D.E., Barone, M.F., Berg, J.C., Resor, B.R., and Lobitz, D.W., "Active Aerodynamic Blade Control Design for Load Reduction on Large Wind Turbines" European Wind Energy Conference, Marseille, France, 26-19 March, 2009.

[12] Berg, D.E., Wilson, D.G., Barone, M.F., Berg, J.C., Resor, B.R., Paquette, J.A., and Zayas, J.R., "The Impact of Active Aerodynamic Load Control on Fatigue and Energy Capture at Low Wind Speed Sites", European Wind Energy Conference, Marseille, France, 16-19 March, 2009.

[13] Berg, D.E., Wilson, D.G., Resor, B.R., Barone, M.F., Berg, J.C., Kota, S. and Ervin, G., "Active Aerodynamic Blade Load Control Impacts on Utility-Scale Wind Turbines", WINDPOWER 2009, Chicago, Illinois, 5-7 May, 2009.

[14] Wilson, Berg, D.E., D.G., Resor, B.R., Barone, M.F., and Berg, J.C., "Combined Individual Pitch Control and Active Aerodynamic Load Controller Investigation for the 5MW UpWind Turbine, WINDPOWER 2009, Chicago, Illinois, 5-7 May, 2009.

[15] NWTC Design Codes (FAST by Jason Jonkman), http://wind.nrel.gov/designcodes/simulators/fast/. Last modified 12-August-2005; accessed 12-August-2005.

[16] NWTC Design Codes (Aerodyn by Dr. David Laino), http://wind.nrel.gov/designcodes/simulators/aerodyn/. Last modified 05-July-2005; accessed 05-July-2005.

[17] IEC TC88-MT1 (ed.). "IEC 61400-1 Ed.3: Wind Turbines – Part 1: Design Requirements", International Electrotechnical Commission, Geneva, 2005.

[18] NWTC Design Codes (Crunch by Marshall Buhl). http://wind.nrel.gov/designcodes/postprocessors/crunch/. Last modified 01-April-2008; accessed 01-April-2008.

[19] Jonkman, J., Butterfield, S., Musial, W., and Scott, G., "Definition of a 5-MW Reference Wind Turbine for Offshore System Development", National Renewable Energy Laboratory, NREL/TP-500-38060, February 2009.

[20] Barlas, T.K., and van Kuik, G.A.M., "Aeroelastic Modelling and Comparison of Advanced Active Flap Control Concepts for Load Reduction on the Upwind 5MW Wind Turbine". European Wind Energy Conference, Marseille, France, 16-19 March, 2009.

[21] Resor, B., Wilson, D., Berg, D., Berg, J. , Barlas, T., and van Kuik, G., "The Impact of Higher Fidelity Models on Active Aerodynamic Load Control Fatigue Damage Reduction", *Proceedings of the 48th AIAA Aerospace Sciences Meeting*, Orlando, FL, January 4-7, 2010.

[22] Wilson, D.G., Resor, B.R, Berg, D.E., Barlas, T.K., and van Kuik, G.A.M., "Active Aerodynamic Blade Distributed Flap Control Design Procedure for Load Reduction on the UpWind 5MW Wind Turbine," *Proceedings of the 48th AIAA Aerospace Sciences Meeting*, Orlando, FL, January 4-7, 2010.

[23] NWTC Design Codes (TurbSim by Neil Kelley and Bonnie Jonkman), http://wind.nrel.gov/designcodes/preprocessors/turbsim/. Last modified 11-September-2008; accessed 11-September-2008.